Analyst

PAPER

View Article Online
View Journal

Cite this: DOI: 10.1039/d6an00122j

Time-domain luminescence lifetime imaging with oxygen sensor particles in the presence of actinic light

Georg Schwendt and Michael Kühl *

Time-gated luminescence lifetime imaging is highly valued in quantitative chemical imaging for its robustness against inhomogeneities in signal intensity and especially background fluorescence, amongst other things. While some literature describes the presence of actinic light during time-gated imaging as problematic, the performance of time-gated imaging in the presence of broadband actinic light remains largely unexplored. To close this knowledge gap, we systematically investigating the influence of broadband actinic light in optical O_2 imaging using water dispersible NIR-emitting O_2 sensor particles with a new open-source, luminescence lifetime imaging system. Mean lifetimes measured *via* time-gated lifetime imaging with properly applied background subtraction showed no influence of actinic light, even at high photon irradiance levels corresponding to mid-day full solar irradiation. Such measurements also showed no sensitivity to background fluorescence with or without actinic light, as long as the background light remained constant in the timeframe of the measurement (~100 ms). We demonstrate the capability of the imaging system for imaging O_2 dynamics during experimental light–dark shifts in biofilms and for intra-tissue O_2 measurements in living corals. The realization of O_2 imaging even under strong actinic light levels, now enables a wide range of applications in environmental, biotechnological and biomedical studies, where beneficial or harmful effects of light treatment are investigated.

Received 1st February 2026,
Accepted 18th March 2026

DOI: 10.1039/d6an00122j

rsc.li/analyst

Introduction

Imaging O_2 concentration in complex environmental samples exposed to luminescent sensor nano- or micro-particles has gained increasing importance in recent years.[1,2] However, substantial interference from high background fluorescence and/or scattering in samples such as biofilms or plant and animal tissues pose a challenge for proper sensor readout, especially with ratiometric imaging approaches (*e.g.* ref. 3). Luminescence lifetime imaging is therefore the preferred imaging modality, where especially time-domain luminescence lifetime imaging can efficiently screen out fluorescence background signals.[4,5] As frequently reported in the literature, it remains, however, a challenge to perform such measurements in the presence of broadband actinic light, especially in light-exposed systems such as phototrophic biofilms and organisms (*e.g.* aquatic plants or animals with photosynthetic symbionts) that exhibit a strong O_2 dynamic. Here changes in actinic light can affect the balance between photosynthesis and respiration in the sample and can potentially interfere with the O_2 imaging procedure (*e.g.* ref. 5 and 6).

In planar sensor applications, interference from background light on sensor performance is typically solved by coating the planar optode with a black, O_2 permeable optical isolation shielding the sensor material from actinic light.[7,8] In applications with transparent sensor foils or dispersed sensor micro- or nano-particles, this is not possible, and here measurements are typically taken immediately after a brief darkening, as a proxy for the O_2 level under the previous light exposure (*e.g.* ref. 6 and 9–11). This can, however, lead to underestimation of the real O_2 dynamic, as even a few seconds of darkening can already lead to strong decline in O_2 in the absence of photosynthesis due to O_2 consumption and diffusion.[12]

While alternative systems have been described in the literature (*e.g.* ref. 13), luminescence lifetime imaging of O_2 in environmental samples has predominantly relied on the use of an imaging system with a modulated CCD camera (SensiCam. SensiMod; Excilitas-PCO GmbH). This system was originally developed by Holst *et al.* (1998),[4] while the imaging software Look@molli was developed by Holst and Grunwald (2001).[14] As this camera is no longer available, there is a strong demand for alternative time-domain luminescence lifetime imaging systems. Only few such systems have been described in recent years,[15–17] and their performance under actinic light remains unknown.

Marine Biology Section, Department of Biology, University of Copenhagen, Strandpromenaden 5, 3000 Helsingør, Denmark. E-mail: mkuhl@bio.ku.dk

In this proof-of-concept study, we re-evaluate the apparent interference of background light in time-domain luminescent lifetime imaging of O_2 reported in the literature (*e.g.* ref. 5 and 6). We show how to overcome this limitation by choosing proper sensing materials and the use of a novel time-domain luminescence lifetime system with proper background compensation.

Experimental

Chemicals

Methyl methacrylate-methacrylic acid copolymer (**PMMA-MA**; 20% methacrylic acid; unspecified MW) was purchased from abcr GmbH (abcr.com); poly(1-vinylpyrrolidone-*co*-styrene) (**PS-VP**; 39% vinylpyrrolidone; 38 wt% emulsion in water; unspecified MW; the properties suggest that this is a block-copolymer[18,19] (not specified by supplier)), poly(styrene-*co*-maleic anhydride) (**PS-MA**; 7% of maleic anhydride; MW 224 000), tetrahydrofuran (THF), acetone and sodium sulfite were acquired from Sigma Aldrich; Pt(II) *meso*-tetra(4-fluorophenyl)tetrabenzoporphyrin (**Pt4F**) was acquired from Porphyrin Systems; low melting point (LMP) agarose (Invitrogen) was purchased from Thermo Fisher Scientific; PBS buffered formalin solution 10% (v/v) was obtained from VWR; N_2 (≥99.8% purity) and O_2 (≥99.5% purity) gas were bought from Air Liquide.

Preparation of optical O_2 sensor particles

Stained **PMMA-MA** and **PS-MA** sensor particles were prepared according to Borisov *et al.* (2009)[20] (method 2c + 3a), while **PS-VP** particles were stained in a THF-water mixture according to Borisov *et al.* (2008),[18] using the respective polymers and the O_2 sensitive indicator **Pt4F** as staining dye.

Cyanobacteria culture

A culture of the cyanobacterium *Acaryochloris marina* was maintained in a vented cap Erlenmeyer cultivation flask in artificial seawater nuetrient medium III (ASN-III)[21] under constant shaking and a defined photon irradiance from white LEDs (50 μmol photons per m^2 per s; 400–700 nm) in a temperature-regulated culture cabinet (ALGAETRON, Photon System Instruments) at 24 °C.

Preparation of sensor particle dispersion containing fixed cyanobacteria

Sea salt was added to 4 mL of 10% (v/v) PBS buffered formalin solution to bring up the salinity to 35, before 4 mL of cyanobacterial culture (with an OD_{780} of 0.322 at a 1 : 20 dilution) was added. After standing for 1 h at room temperature the fixed cell dispersion was centrifuged, decanted and redispersed in 4 mL sea water. This procedure was repeated thrice, but in the last step the centrifuged cells were redispersed in 3.6 mL sea water before 400 μL of 10 g L^{-1} **PS-VP** sensor particle dispersion was added. The dispersion was used for calibration immediately afterwards, and therefore prepared twice, with adjusted volume of cell culture (determined by optical density) to match the first dispersion.

Preparation of the cyanobacterial biofilm

1.6 mL of 10 g L^{-1} **PMMA-MA** sensor particle dispersion was adjusted to salinity 35 by addition of sea salt before 64 mg of LMP agarose were added and the mixture was heated to 70 °C until LMP agarose completely melted. The mixture was cooled down to 37 °C before 1.6 mL of pre-heated (37 °C) *Acaryochloris marina* cell culture (with an OD_{780} of 0.322 at a 1 : 20 dilution) was added. After mixing, the bioink was spread on a Petri dish, resulting in a *ca.* 0.5 mm thick gel layer. After gelation, ASN-III medium was added and the bio gel was incubated for 14 days under a defined photon irradiance from white LEDs (50 μmol photons per m^2 per s; 400–700 nm) in a temperature-regulated culture cabinet (ALGAETRON, Photon System Instruments) at 24 °C, where the medium was exchanged weekly.

Sampling of tropical corals

Small colony fragments of the reef-building coral *Pocillopora damicornis* were collected from the reef-flat off Heron Island (Great Barrier Reef, Australia) and were maintained at Heron Island Research Station in shaded outdoor aquaria flushed with fresh reef water prior to experiments.

Light sources and light related measurements

A fiber-optic, white LED lamp (KL 2500LED, Schott GmbH, see Fig. S1 for emission spectrum) was used as an actinic light source for illuminating samples with defined photon irradiance of photosynthetically active radiation (PAR; 400–700 nm), as determined with spherical micro quantum sensor connected to a light meter (US-SQS/L and ULM-500, WALZ GmbH). Emission spectra were recorded on a calibrated spectroradiometer (BTS256-EF, Gigahertz-Optik GmbH). In most experiments, sensor particles were excited with a high-power LED system (LPS3, iLA_5150 GmbH) mounted with a red LED (612 nm) and equipped with a liquid light guide. For comparison of calibration curves obtained with time-domain and frequency-domain camera systems, we used the red LED (625 nm) channel of a multichannel light engine (LEDHub, Omicron GmbH), which also was equipped with a liquid light guide. LED fall times were measured with a fast photodiode detector (PDA10A2; Thorlabs GmbH) connected to an oscilloscope (SDS824X HD; Siglent) *via* a 50 Ohm feedthrough terminator. All imaging was performed in a temperature-controlled room at 26 °C.

Time-domain lifetime imaging

For time-domain luminescence lifetime imaging, we assembled an imaging system similar to a recently published CMOS camera-based setup[17] for rapid lifetime determination (RLD), which we controlled *via* a newly developed custom-build software, including a graphical user interface. Our setup (Fig. S2) consists of a monochrome CMOS camera (4112 × 3008 pixels) capable of time-gated, multi-exposure imaging

(MC124MG-SY-UB; Ximea) operated with 2 × 2 binning at full resolution, an external excitation light source (see above), and a microcontroller board (Uno rev3; Arduino) for timing control of the camera and excitation light source trigger pulses. Additionally, an optional 12-bit digital to analog (DAC) module (Gravity I2C 12-Bit DAC module; DFRobot) can be used to control the light intensity of the excitation light source, while the actinic light source can be controlled by a Python script when connected *via* a USB port to the image acquisition PC. Acquisition time stamps are saved alongside images to allow precise determination of acquisition time of each image. The camera was equipped with a color-corrected (400–1000 nm) c-mount objective (Xenoplan 1.4/17; Schneider-Kreuznach GmbH) with a mounted long pass-filter. The filter LP765 HT (Schneider-Kreuznach GmbH) was used in most experiments, while the LP695 HT filter (Schneider Kreuznach GmbH) was used in the comparison of calibration curves obtained with the time-domain and frequency-domain imaging systems, respectively. The software to control the time-gated imaging setup (including a description of the settings) is freely available at https://github.com/MicroEnvironment/Lifetime-imaging-in-actinic-light. Settings: exposure time 20 µs, excitation pulse width 40 µs, delay 1: 2.5 µs (see Fig. S3b for fall time of LPS3 excitation light source with red LED), delay 2: 22.5 µs, exposures per frame: variable depending on signal intensity.

Frequency-domain lifetime imaging

Frequency-domain luminescence lifetime imaging was done with a pco.flim camera (PCO-Excilitas GmbH), which directly controlled the excitation light source (LEDHub light engine; Omicron Laserage) using a custom-made software available at https://github.com/ZariaFerte/CameraPCO_FLIM_software. Imaging was performed with the following settings in the software: wave form: rectangular; number of phases: 4; symmetry correction: twice; phase order: opposite; selected tap: both; background correction: yes; frequency (Hz): 4000. The exposure time was set to 0.01 s but was decreased when saturation was reached. A detailed explanation of the settings and how they translate into the modulation scheme can be found in the user manual of the commercially available pco.flim camera (https://www.excelitas.com/sites/default/files/assets/product/document/26559.pdf).

Oxygen calibrations

Unless otherwise noted, sensor particle dispersions for calibration had a sensor particle concentration of 0.5 g L^{-1}. The measurement setup consisted of a quartz cuvette with 1 cm optical path length (Hellma Analytics), which was faced directly by the camera. The actinic light source and excitation light source faced the cuvette at an ~45° angle from the side and above, respectively. The photon irradiance of the actinic light source was measured in water prior to calibration measurements at a spot close to the reference O_2 and temperature sensors (OXR50-OI and TSUB21, Pyroscience GmbH), which were read-out by a FireSting GO2 meter (Pyroscience GmbH) and calibrated according to the manufacturer's recommendations.

Calibration values (mean pO_2 and standard deviation) were obtained in the same ~100 × 100 pixel ROI of images to avoid deviations from both reference pO_2 values and photon irradiance. Calibrations were started at the highest O_2 level (in the case of **PMMA-MA** sensor particles, hyperoxic levels were reached by purging the calibration dispersion with O_2 gas), and successively lowered O_2 levels were reached by intermittent purging the calibration dispersion with N_2 gas. Once the desired pO_2 value was reached, purging was paused by removing the gas inlet from the cuvette, and calibration points were taken in quick succession at different photon irradiance levels from the actinic light source. For the last calibration point (anoxic) a spatula tip of sodium sulfite was dissolved in the calibration dispersion prior to imaging. The average accuracy (in the range of 0–200 hPa) is reported as the root-mean-square error (RMSE). Calibration coefficients were derived from a least-squares fit of the combined data from calibration runs at a photon irradiance of 0, 500 and 1000 µmol photons per m^2 per s. To validate the model, these coefficients were then applied to the independent calibration data set acquired at 2000 µmol photons per m^2 per s to assess the deviation.

Imaging of O_2 in biofilm

A Petri dish containing the biofilm sample was imaged vertically from above by the camera *via* the objective and 765 HT long-pass emission filter, while the light guides form both the actinic light source and the excitation light source were facing the biofilm at a 45° angle from above (see Fig. S4). The intensity setting on the actinic light source to reach a photon irradiance of 200 µmol photons per m^2 per s (±10% due to inhomogeneous illumination over the biofilm) was determined in advance. A script was used to synchronize image acquisition relative to switching the actinic light on or off. Three light/dark cycles of 90 min each were recorded, and images were acquired more frequently at the beginning of each cycle (1 min intervals) than at later stages of each cycle (2, 5, 10 min intervals).

Imaging of O_2 in tropical corals

We imaged the internal O_2 conditions in the reef-building coral *Pocillopora damicornis*, *via* injection of optical O_2 sensor particles into the gastrovascular cavity of the coral using procedures described by Kühl *et al.* (2024).[22] To ensure more controlled injection of sensor particles, the coral was intermittently sedated for a few minutes in seawater with $MgCl_2$ (92 mM), before the injection of ~3 µL **PS-VP** sensor particles (10 g L^{-1}) into the gastrovascular cavity of individual coral polyps. After injection, the coral sample was moved to a laminar flow chamber (see ref. 22) flushed with aerated seawater at 26 °C, where it was allowed to recover for 30 min in the dark before onset of experiments. Since cnidarians are known to quickly recover (within seconds or minutes) after the removal of Mg^{2+},[23] the use of $MgCl_2$ as sedative during injec-

tion is unlikely to significantly influence the following oxygen measurements 30 minutes after removal.

The coral sample was imaged by the camera system (with an additional 0.5 mm distance ring to increase magnification) vertically from above, while actinic and excitation light was provided at ~35° (due to decreased working distance), *i.e.*, a similar measuring geometry as in the biofilm experiments. The coral was imaged 5 times in the dark in intervals of 1 minute, before actinic light (50 μmol photons per m^2 per s;400–700 nm) was switched on and the coral was imaged with increasing time intervals (10 s, 30 s, 1 min) during a 9 min time period.

Data analysis

The rapid lifetime determination (RLD) method typically uses two frames (or "windows") with equal exposure time, which are recorded at different delays after an excitation light pulse (see ref. 17 for a detailed description of the RLD scheme with CMOS-cameras). A "dark" frame with the same pulsing scheme as window 1 is acquired without excitation light pulses to correct the (constant) background (most importantly from the actinic light) from windows 1 and 2 according to eqn (1):

$$I_{x,\mathrm{corr}} = I_x - I_{\mathrm{dark}} \quad x = 1, 2. \tag{1}$$

The time delay, Δt, between these image frames and their integrated luminescence intensity ratio can be used to calculate the lifetime with eqn (2)

$$\tau = \frac{\Delta t}{\ln\left(\frac{I_{1,\mathrm{corr}}}{I_{2,\mathrm{corr}}}\right)}. \tag{2}$$

It should be noted that for eqn (2) to yield the correct lifetime, the signal needs to be mono-exponential. Since luminophores embedded in polymer matrices generally do not show a mono-exponential decay,[24] the calculated lifetimes are "apparent lifetimes", which are provided for better comparability among studies. The analytical information is in the ratio of $I_{1,\ \mathrm{corr}}/I_{2,\ \mathrm{corr}}$, and the determination of absolute lifetimes is not necessary for chemical sensing.[25]

Calibration curves were measured by performing RLD imaging with sensor particles kept at different pO_2 levels and constant temperature. The calibration curves were fitted by the two-site model,[24] which assumes that the indicator is present in two different microenvironments with different gas permeabilities within the host polymer, where one compartment shows negligible O_2 quenching:

$$\frac{\tau}{\tau_0} = \frac{f}{1 + K_{\mathrm{sv}} \cdot \mathrm{pO_2}} + (1 - f) \tag{3}$$

here K_{SV} is the Stern–Volmer constant, pO_2 is the oxygen partial pressure and f is the distribution factor between the two sites, *i.e.*, the quenchable fraction of the indicator.

The calibration curves (obtained at experimental temperature) were then used to calculate pO_2 images (see Results and Discussion section). We note that in the presence of actinic light, the "dark" frame can often also be used to obtain structural information.

Results and discussion

A new, flexible time-domain luminescence lifetime imaging system

Our imaging system builds on a recently introduced CMOS camera-based luminescence lifetime imaging setup,[17] which we improved by implementing precise timing controls of trigger pulses within 1 clock cycle of the used microcontroller board (62.5 ns for the Arduino Uno Rev3@16 MHz) (see Experimental). The improved timing control is *e.g.* useful for accurately timing trigger pulses of both camera and excitation source to reach optimal signal intensity with minimal background, while considering the fall times of the excitation source and background fluorescence. We also implemented the possibility to control external light sources for actinic light relative to programmable image acquisition sequences. Additionally, an optional DAC module can be used to control the excitation light intensity. Finally, we made the imaging system more accessible and user-friendly by including a graphical user interface (Fig. S5). The lifetime imaging system can be used to image lifetimes of 10 μs and above due to the minimum exposure time of the camera (19 μs) and fall time of the excitation light source (2.5 μs).

Here we focused on developing a robust and flexible imaging system for time-domain luminescence lifetime imaging based on rapid lifetime determination. However, timing schemes of other imaging techniques like (i) frame-straddling enabling rapid luminescence lifetime proportional O_2 imaging,[26] which is especially useful for combined imaging of flow and O_2 around aquatic systems and organisms, or (ii) imaging schemes reconstructing the whole phosphorescence decay curve,[16] can be used either directly (frame-straddling) or after minor modifications of the present software platform.

Influence of actinic light on O_2 imaging

The influence of broadband actinic light on time-gated luminescence lifetime imaging was first investigated by calibrating three different O_2 sensor particle dispersions, all based on the indicator **Pt4F** (see Experimental). Each pO_2 data point was recorded at a photon irradiance of photosynthetically active radiation (PAR; 400–700 nm), E_d(PAR), of 0, 500, 1000 and 2000 μmol photons per m^2 per s. The resulting data points and averaged calibration curves (over all four datasets per material) are shown in Fig. 1.

The obtained calibration parameters for all investigated materials are summarized in Table 1 and are comparable to those found in literature for **Pt4F** in **PMMA-MA**[22] as a direct comparison, and **Pt4F** in polystyrene foil[27] as a comparison for PS based particles **PS-VP** and **PS-MA**. While the precision (1σ) of a single lifetime measurement was 3% of the lifetime value for all materials (corresponding to ~10 hPa), the average accuracy varied depending on the material between 2 and 7 hPa

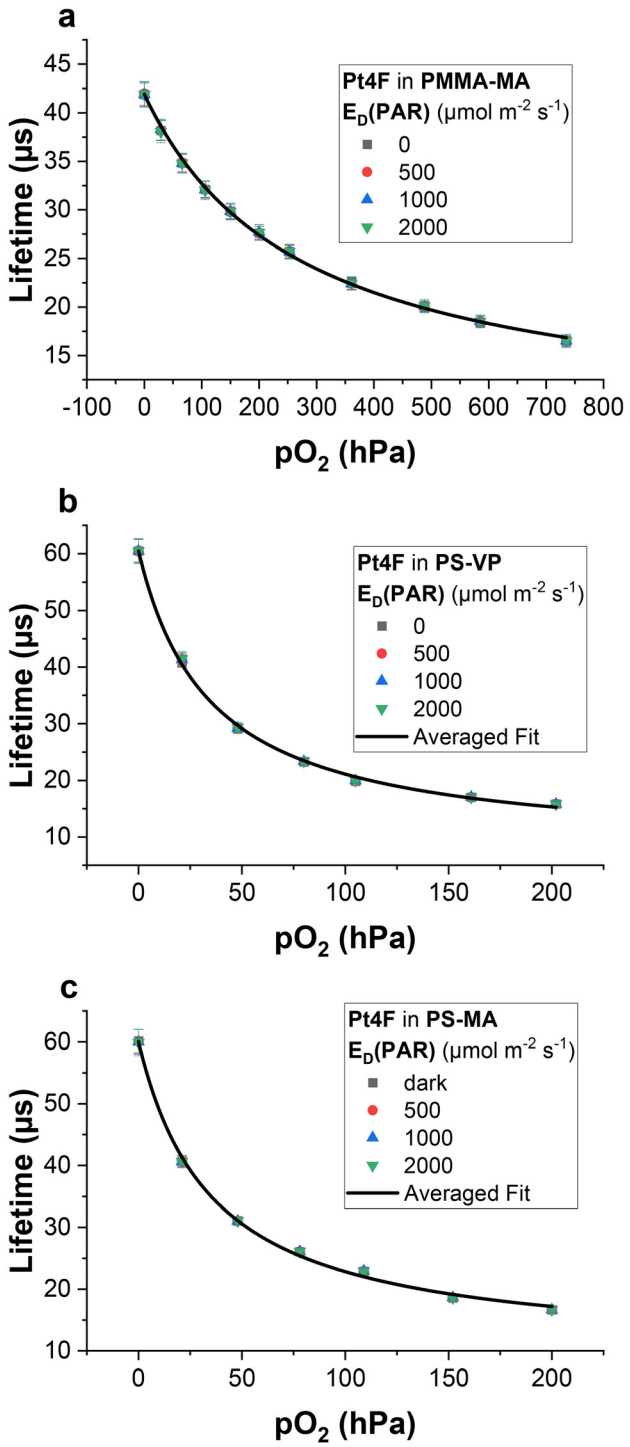

Fig. 1 Calibration curves obtained under different photon irradiance levels (400–700 nm; units of µmol photons per m^2 per s) for **Pt4F** in: **PMMA-MA** (a), **PS-VP** (b) and **PS-MA** (c) sensor particles. Example calibration images for **PS-VP** O_2 sensor particles can be found in Fig. S6.

across the pO_2 range of 0–200 hPa (*cf.* Table 1). The analytical repeatability (precision of the mean) was below 1 hPa for all investigated materials across the pO_2 range of 0–200 hPa. The photostability of the indicator **Pt4F** in PS[27] and PMMA-MA[22]

Table 1 Calibration parameters obtained for the investigated optical O_2 sensing materials, *i.e.*, different nanoparticles containing the O_2 indicator **Pt4F**

Sensing particles	K_{SV} [h Pa^{-1}]	f	T_0 [µs]	Accuracy$_{(0–200\ hPa)}$ [hPa]
PMMA-MA	0.0037	0.82	42	2
PS-VP	0.0289	0.88	61	6
PS-MA	0.0280	0.84	60	7

matrices was previously found to be excellent and moderate, respectively. Since the time under excitation light is low (typically in the low ms range), the main contribution to photobleaching is due to the actinic light irradiation, which is expected to be maintainable for hours without significant effect on the results under high (E_d(PAR) of 2000 µmol photons per m^2 per s) and moderate photon irradiance (E_d(PAR) < 300 µmol photons per m^2 per s) with PS based particles and PMMA-MA particles, respectively.

Despite previous claims that even low levels of ambient light could influence the measured lifetimes[5,6] in time-domain imaging with the system of Holst *et al.*,[4] our calibrations showed that even very strong broadband actinic light of up to a E_d(PAR) levels of 2000 µmol photons per m^2 per s, *i.e.*, light levels equivalent to mid-day full solar irradiation, had no influence on measured lifetimes when an appropriate simple background subtraction was applied. Surprised by this stark contrast, we tried to reproduce the results of one of the mentioned publications,[5] which also employs background subtraction.

We found that the discrepancy arose from an incorrectly applied gating scheme for the "dark" frame, which is used for background subtraction in the look@moli software.[14] Careful characterization of the gating scheme by an oscilloscope, when measuring with the system of Grunwald and Holst,[14] showed that gating was apparently not applied during the integration period of the "dark" image at all. This resulted in a "dark" image with intensities multiple times higher than they should be. By bypassing the trigger box and implementing the correct gating scheme into the camera system, we were able to obtain calibration curves matching the results of the calibration with our new camera system setup (Fig. S7).

However, even with the new time-domain luminescence lifetime camera system described here, it should be noted that the intensity of the actinic light must not change significantly during the acquisition time frame (~100 ms), and that the usable dynamic range of the camera decreases with increasing actinic light intensity. It is therefore necessary to use an excitation light source, which is significantly stronger than the actinic light source, and advisable to employ an O_2 indicator that is significantly red shifted from the primary wavelength range of the actinic light source. Even under these conditions, it should be kept in mind that using too high excitation light intensity can result in errors due to the depopulation of the ground state.[28] In our study, the absence of such an effect was easily confirmed by comparing measurements taken at

different excitation light intensities. Furthermore, although the total time under excitation light illumination is low (typically in the low millisecond range per measurement), effects of phototoxicity[29] in biological and medical applications can require lower excitation light intensities to be used. This decrease in excitation light intensity in turn decreases the maximum photon irradiance that can be used as actinic light to maintain a favorable signal to noise ratio. While the prerequisite for constant actinic light can be easily met under laboratory conditions which entail most applications, this is not the case in outdoor environments where *e.g.* clouding,[30] sunflecks or water wave-lensing[31] can dramatically change the actinic light irradiance on a sub-second timescale, which makes the current method unsuitable for such applications.

Influence of background fluorescence and comparison to frequency-domain lifetime measurements

To prove that the RLD method, as implemented in our new time-domain luminescence lifetime camera system, remains unaffected by background fluorescence even in the presence of broadband actinic light, we performed calibration experiments with O_2 sensor particle suspensions that additionally contained fixed cells of the chlorophyll *d*-rich cyanobacterium *Acaryochloris marina* showing maximal *in vivo* Chl *d* fluorescence at 700–750 nm.[32] Here we used a 695 nm long-pass emission filter (instead of the 765 nm long-pass filter) to allow more fluorescence background to reach the detector. As comparison, the same experiment was also performed with a frequency-domain lifetime imaging camera, which are known to be prone to background fluorescence.[5] We found no influence of background fluorescence on the measured lifetimes with the time-domain camera system (Fig. 2a), while the frequency-domain camera system exhibited a systematic error of lowered lifetimes in the presence of background fluorescence (Fig. 2b). Broadband actinic light had no effect on the measured mean lifetimes for both cameras, as long as the usable dynamic range of the cameras was not too low as result of the background signal. Consequently, no calibration curve above 200 μmol photon per m^2 per s could be obtained with the frequency-domain camera due to an overwhelming background signal, while the time-domain camera system could handle tenfold higher photon irradiance levels, with increased standard deviation being the only limitation. While both methods are generally affected in the same manner, *i.e.*, a decrease in usable dynamic range and signal to noise ratio due to an added offset signal, the effect is more pronounced for the frequency domain system because of instrumental demodulation of the analytical signal due to finite gate width, and additional noise, which is captured from the presence of light on the QMFLIM2 CMOS image sensor of the PCO.FLIM camera during readout.[33]

Nevertheless, since background light decreases the usable dynamic range of the camera, and chlorophyll fluorescence in living organisms is not constant,[34,35] it is advisable to use NIR emitting O_2 indicators in combination with long-pass emission filters that filter out the chlorophyll fluorescence. Here, the used combination of **Pt4F** and a 765 nm LP filter screens out most of the chlorophyll fluorescence and is suitable for most applications. However, for certain use cases (*e.g.* low-light with strong chlorophyll background) longer emitting O_2 indicators such as platinum(II) aza-benzoporphyrins[36] may be a more suitable indicator choice.

Imaging O_2 in a photosynthetic biofilm

As a first example of application, we imaged the O_2 dynamics in an artificial biofilm of the cyanobacterium *Acaryochloris marina* immobilized in an agarose hydrogel slab containing O_2 sensor nanoparticles (**Pt4F** in **PMMA-MA**). Such application is representative for lifetime imaging-based O_2 sensing in biofilms, tissues and bioprinted cell constructs, where O_2 sensor particles can either be immobilized onto sample surfaces, *e.g.* ref. 10 and 11, or incorporated in hydrogels to functionalize the bioink with immobilized cells.[37,38] Of the sensor materials investigated in the present study, **PMMA-MA** was found most

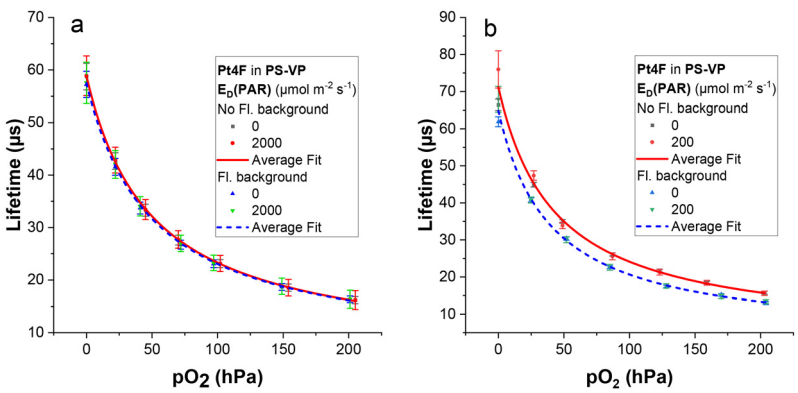

Fig. 2 Calibration curves of luminescence lifetime of **PS-VP** particles as a function of O_2 partial pressure, pO_2, as obtained with the new time-domain camera system (a) and a commercial frequency domain camera system (b). Calibration curves were measured in the absence and presence of background fluorescence at varying levels of actinic light intensity quantified as photon irradiance (400–700 nm) in units of μmol photons per m^2 per s (measurement points at 500 and 1000 μmol photons per m^2 per s are not shown in (a) for visibility).

suitable for this purpose due to its lower sensitivity towards O_2, enabling accurate measurements over a wider range of O_2 concentrations above air saturation, as compared to the polystyrene based alternatives (Table 1 and Fig. 1).

We could image the dynamic changes of O_2 concentration at the surface of the cyanobacterial biofilms during experimental light dark cycles, showing rapid built up of O_2 in the biofilm due to cyanobacterial photosynthesis in light, and rapid depletion of O_2 in the dark due to respiration of the cells (Fig. 3). Steady state O_2 concentrations in the biofilm, reflecting a balance between photosynthetic production, respiratory consumption and diffusional transport of O_2, reached super saturating levels of ~400 hPa pO_2 after 45 min, and sub-saturation levels of ~150 hPa pO_2, after 90 min in darkness. Regional inhomogeneity can be seen when looking at "steady state" O_2 images acquired under darkness and light, respectively, (Fig. 4), hinting at an inhomogeneous distribution of cells within the agarose gel. Similar light–dark dynamics have been found in lifetime-imaging of O_2 in 3D bioprinted constructs of the green microalga *Chlorella sorokiniana* UTEX1230 cells in GelMA,[38] albeit this study quantified O_2 in the light by briefly switching actinic light off prior to image acquisition, which limited the temporal resolution in their measurements and underestimated the real O_2 levels and dynamic under illumination. In our measurements, the employed imaging method had a temporal resolution of 10 Hz (with 2 × 2 binning). In principle, this allows for accurate imaging of much faster O_2 dynamics, *e.g.* as observed in corals[39] or microbial mats.[40]

Subsurface O_2 imaging in animal tissue

A second application example of the new imaging system involved the use of O_2 sensor nanoparticles, that were injected into the gastric cavity of reef-building corals following pro-

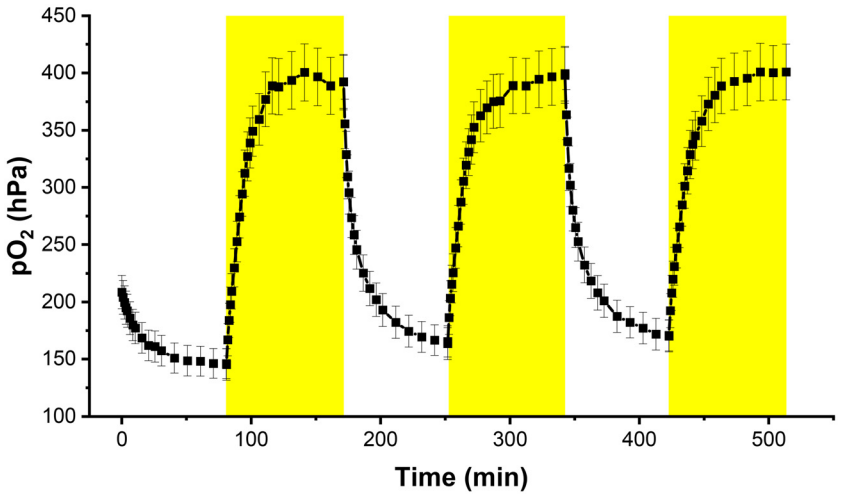

Fig. 3 Temporal dynamics of pO_2 during light and dark cycles in a randomly chosen ROI (with an area of 2.6 mm^2, see black square in Fig. 4) of an artificial biofilm of the cyanobacterium *Acaryochloris marina* in agarose. Yellow highlighted areas in the graph correspond to active actinic illumination with a photon irradiance (400–700 nm) of 200 μmol photons per m^2 per s, while data points outside highlighted area were recorded in the absence of actinic light, *i.e.* darkness.

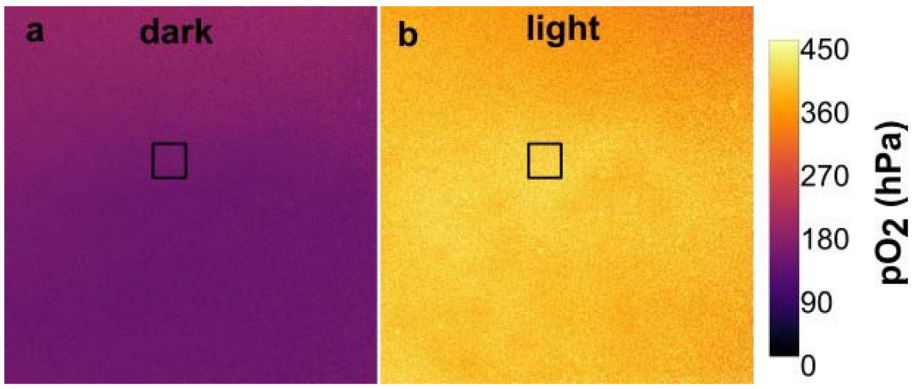

Fig. 4 Steady state pO_2 in a rectangular section of the agarose gel in darkness (a) and under actinic illumination with a photon irradiance (400–700 nm) of 200 μmol photons per m^2 per s (b). The black rectangle represents the ROI used for plotting the pO_2 profile in Fig. 3.

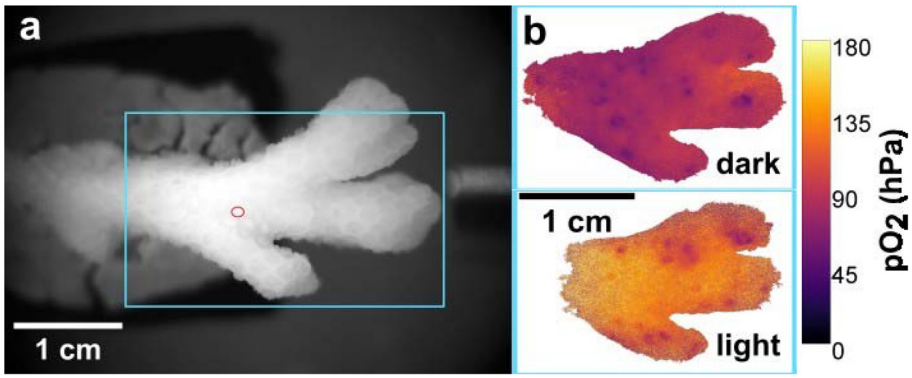

Fig. 5 Monochrome picture of an imaged fragment of the coral species Pocillopora damicornis showing ROIs (blue rectangle and red ellipse) (a) and the corresponding pO_2 images in the blue ROI, as measured in the dark (b, top) and under actinic illumination at a photon irradiance (400–700 nm) of 50 μmol photons per m^2 per s (b, bottom). See Fig. 6 for illumination scheme and timeline of the image acquisition.

cedures of Kühl *et al.* (2024).[22] Such application is representative of intra-tissue O_2 measurements, which are highly relevant both in environmental and biomedical applications such as *e.g.* imaging of hypoxia in tumors and organoids.[41,42]

Two example pO_2 images taken in darkness and under actinic light, respectively, showcase the internal pO_2 distribution in a coral fragment (Fig. 5b), showing significantly lower pO_2 under darkness due to coral respiration (~80 hPa), as compared to the pO_2 distribution under actinic light when the algal symbionts of the coral produce O_2 *via* their photosynthesis (~140 hPa). Our images also show pronounced lateral inhomogeneities in pO_2, revealing a complex O_2 distribution within the coral tissue, which cannot be resolved *e.g.* by point measurements of microsensors.

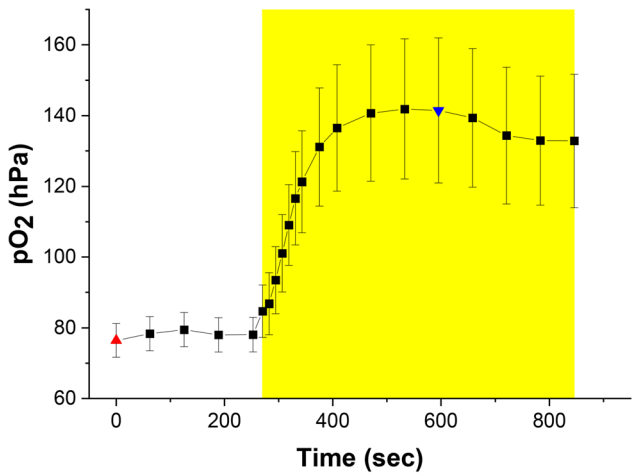

Fig. 6 Temporal change of pO_2 in a tissue area with a single coral polyp animal (red ellipse in Fig. 5a). The yellow highlighted area in the graph corresponds to active actinic illumination with a photon irradiance (400–700 nm) of 50 μmol photons per m^2 per s, while data points outside highlighted area were recorded in the absence of actinic light, *i.e.*, darkness. Red and blue triangular data points show acquisition time of pO_2 images in Fig. 5b (top and bottom, respectively).

The integrated temporal changes in pO_2 in a ROI equivalent to a single coral polyp animal (red ellipse in Fig. 5a) is shown in Fig. 6. From an initial value of ~80 hPa in darkness, the pO_2 quickly increased upon exposure to actinic light, reaching a steady state value of ~140 hPa after 5 min. Similar fast O_2 dynamics have been demonstrated by point measurements with fast-responding O_2 microsensors in coral tissues.[39]

Conclusion

In conclusion, we demonstrate a simple method for O_2 imaging in the presence of broadband actinic light illumination using a new, modular time-domain luminescence lifetime imaging system. While the method requires that the actinic light source emits at a constant light intensity (within the ~100 ms time frame of a measurement), and that the excitation light source is significantly brighter than the actinic light source, these requirements are easily met under laboratory conditions. Measurements with the presented lifetime imaging system remain immune to background fluorescence in the presence of actinic light and tolerate much higher actinic light intensities than camera systems for frequency-domain lifetime imaging. This now enables a wide range of O_2 imaging applications with light exposed samples in environmental and biotechnological studies of photosynthetic systems and organisms, as well as in biomedical studies, where *e.g.* the effect of light treatments on the O_2 dynamics in cells and tumors can now be directly monitored. While the lifetime imaging method in the presence of actinic light was demonstrated only for O_2, the method would also work for other parameters (*e.g.* pH or temperature) when used with compatible optical sensor materials.

Conflicts of interest

The authors declare no conflicts of interests.

Data availability

The datasets generated and analyzed during the current study are available from the corresponding author upon reasonable request.

Supplementary information (SI): Supplementary figures (S1–S7). See DOI: https://doi.org/10.1039/d6an00122j.

All software described in the current study is open source (under a GNU license) and is freely available at: https://github.com/MicroEnvironment/Lifetime-imaging-in-actinic-light.

Acknowledgements

This study was supported by the Gordon and Betty Moore Foundation (grant no. GBMF9206; https://doi.org/10.37807/GBMF9206; MK) and the Villum Foundation (VIL 50371; MK). The coral work in this study was done under the permit G24/49877.1 granted by the Great Barrier Reef Marine Parks Authorities. We thank Sergey Borisov and Sing Teng Chua for helpful discussions and for providing sensor materials and the *A. marina* culture, respectively. Sofie Lindegaard Jakobsen is thanked for general technical assistance. The staff at Heron Island Research Station are thanked for their outstanding assistance during the field work.

References

1 K. Koren and M. Kühl, in *Quenched-phosphorescence Detection of Molecular Oxygen: Applications in Life Sciences*, ed. D. B. Papkovsky and R. I. Dmitriev, The Royal Society of Chemistry, 2018, pp. 145–174.
2 M. Moßhammer, K. E. Brodersen, M. Kühl and K. Koren, *Microchim. Acta*, 2019, **186**, 126.
3 Z. Bognár, M. Mosshammer, K. E. Brodersen, E. Bollati, R. E. Gyurcsányi and M. Kühl, *ACS Sens.*, 2024, **9**, 1763–1774.
4 G. Holst, O. Kohls, I. Klimant, B. König, M. Kühl and T. Richter, *Sens. Actuators, B*, 1998, **51**, 163–170.
5 K. Koren, M. Moßhammer, V. V. Scholz, S. M. Borisov, G. Holst and M. Kühl, *Anal. Chem.*, 2019, **91**, 3233–3238.
6 M. Kühl, G. Holst, A. W. D. Larkum and P. J. Ralph, *J. Phycol.*, 2008, **44**, 541–550.
7 R. N. Glud, M. Kühl, O. Kohls and N. B. Ramsing, *J. Phycol.*, 1999, **35**, 270–279.
8 J. Santner, M. Larsen, A. Kreuzeder and R. N. Glud, *Anal. Chim. Acta*, 2015, **878**, 9–42.
9 M. Kühl, E. Trampe, M. Mosshammer, M. Johnson, A. W. Larkum, N.-U. Frigaard and K. Koren, *eLife*, 2020, **9**, e50871.
10 J. Fabricius-Dyg, G. Mistlberger, M. Staal, S. M. Borisov, I. Klimant and M. Kühl, *Mar. Biol.*, 2012, **159**, 1621–1631.
11 K. Elgetti Brodersen, M. Kühl, E. Trampe and K. Koren, *Plant J.*, 2020, **104**, 1504–1519.
12 R. N. Glud, N. B. Ramsing and N. P. Revsbech, *J. Phycol.*, 1992, **28**, 51–60.
13 K. Oguri, H. Kitazato and R. N. Glud, *Mar. Chem.*, 2006, **100**, 95–107.
14 G. Holst and B. Grunwald, *Sens. Actuators, B*, 2001, **74**, 78–90.
15 R. Sen, L. M. Hirvonen, A. Zhdanov, P. Svihra, S. Andersson-Engels, A. Nomerotski and D. Papkovsky, *Biomed. Opt. Express*, 2020, **11**, 77–88.
16 A. Goncharov, Z. Gorocs, R. Pradhan, B. Ko, A. Ajmal, A. Rodriguez, D. Baum, M. Veszpremi, X. Yang, M. Pindrys, T. Zheng, O. Wang, J. C. Ramella-Roman, M. J. McShane and A. Ozcan, *ACS Nano*, 2024, **18**, 23365–23379.
17 G. Rousseau, M. Pons, H. Adelerhof, N. Pellerin, M. Giesbergen, B. Carde, M. Wolff, K. Blanckaert, S. M. Borisov and B. Fond, *Sens. Actuators, B*, 2026, **447**, 138849.
18 S. M. Borisov, T. Mayr and I. Klimant, *Anal. Chem.*, 2008, **80**, 573–582.
19 R. Nagarajan, M. Barry and E. Ruckenstein, *Langmuir*, 1986, **2**, 210–215.
20 S. M. Borisov, T. Mayr, G. Mistlberger, K. Waich, K. Koren, P. Chojnacki and I. Klimant, *Talanta*, 2009, **79**, 1322–1330.
21 R. Rippka, J. Deruelles, J. B. Waterbury, M. Herdman and R. Y. Stanier, *Microbiology*, 1979, **111**, 1–61.
22 M. Kühl, D. A. Nielsen and S. M. Borisov, *ACS Sens.*, 2024, **9**, 4671–4679.
23 S. Arossa, S. G. Klein, A. J. Parry, M. Aranda and C. M. Duarte, *Front. Mar. Sci.*, 2022, **9**, 870832.
24 J. N. Demas, B. A. DeGraff and W. Xu, *Anal. Chem.*, 1995, **67**, 1377–1380.
25 M. Schäferling, *Angew. Chem., Int. Ed.*, 2012, **51**, 3532–3554.
26 S. Ahmerkamp, C. O. Pacherres, M. Mosshammer, M. Godefroid, M. Wind-Hansen, M. Kuypers, L. Behrendt, K. Koren and M. Kühl, *ACS Sens.*, 2024, **9**, 5531–5540.
27 S. M. Borisov, G. Nuss and I. Klimant, *Anal. Chem.*, 2008, **80**, 9435–9442.
28 C. Larndorfer, S. M. Borisov, P. Lehner and I. Klimant, *Analyst*, 2014, **139**, 6569–6579.
29 J. Icha, M. Weber, J. C. Waters and C. Norden, *BioEssays*, 2017, **39**, 1700003.
30 W. B. Mol, W. H. Knap and C. C. van Heerwaarden, *Earth Syst. Sci. Data*, 2023, **15**, 2139–2151.
31 C. J. Veal, M. Carmi, G. Dishon, Y. Sharon, K. Michael, D. Tchernov, O. Hoegh-Guldberg and M. Fine, *J. Exp. Biol.*, 2010, **213**, 4304–4312.
32 Z. Petrášek, F.-J. Schmitt, C. Theiss, J. Huyer, M. Chen, A. Larkum, H. J. Eichler, K. Kemnitz and H.-J. Eckert, *Photochem. Photobiol. Sci.*, 2005, **4**, 1016–1022.
33 R. Franke and G. A. Holst, in *Imaging, Manipulation, and Analysis of Biomolecules, Cells, and Tissues XIII*, SPIE, 2015, vol. 9328, p. 93281K.
34 L. Nedbal, J. Soukupová, D. Kaftan, J. Whitmarsh and M. Trtílek, *Photosynth. Res.*, 2000, **66**, 3–12.
35 N. R. Baker, *Annu. Rev. Plant Biol.*, 2008, **59**, 89–113.
36 S. M. Borisov, G. Zenkl and I. Klimant, *ACS Appl. Mater. Interfaces*, 2010, **2**, 366–374.

37 E. Trampe, K. Koren, A. R. Akkineni, C. Senwitz, F. Krujatz, A. Lode, M. Gelinsky and M. Kühl, *Adv. Funct. Mater.*, 2018, **28**, 1804411.
38 S. Murthy, M. Mosshammer, E. Trampe and M. Kühl, *Biofabrication*, 2025, **17**, 045010.
39 M. Kühl, Y. Cohen, T. Dalsgaard, B. Jørgensen and N. Revsbech, *Mar. Ecol.: Prog. Ser.*, 1995, **117**, 159–172.
40 E. H. G. Epping, A. Khalili and R. Thar, *Limnol. Oceanogr.*, 1999, **44**, 1936–1948.
41 D. B. Papkovsky and R. I. Dmitriev, *Cell. Mol. Life Sci.*, 2018, **75**, 2963–2980.
42 A. C. Debruyne, I. A. Okkelman, N. Heymans, C. Pinheiro, A. Hendrix, M. Nobis, S. M. Borisov and R. I. Dmitriev, *ACS Nano*, 2024, **18**, 12168–12186.